Supporting Information template

Please use this template when formatting and submitting your Supporting Information.

This template serves as both a "table of contents" for the supporting information for your article and as a summary of files.

Once you have completed this template, you should delete this instruction page.

Overview

Please note that all supporting information will be peer reviewed with your manuscript. For more information, please see the Supporting Information Guidelines in Author Resources

Using this Template

Type or paste the appropriate text (title, author list, and corresponding authors) into the template below.

Contents of this document:

- All Supporting text and figures should be included in this document.
- Movie files and audio files should be uploaded separately, following AGU naming conventions. File name and descriptions for these should be included in this template.
- All references should be included in the reference list of the main paper so that they can be indexed, linked, and counted as citations. The reference section does not count toward length limits.

How to fill out this document:

- Insert supporting information content into each appropriate section of the template.
- Figures should appear above each caption.
- To add additional captions, simply copy and paste each sample caption as needed.
- You will be prompted to upload these files on the Upload Files tab during the submission process, using file type "Supporting Information (SI)"
- Data (displayed in tables) should only be shared in the Supporting Information section for the sole purpose of peer review.

Journal of Geophysical Research: Planets

Supporting Information for

Geometry of Freezing Impacts Ice Composition: Implications for Icy Satellites

J. J. Buffo[1], C. R. Meyer[1], C. J. Chivers[2, 3], C. C. Walker[3], C. Huber[4] and B. E. Schmidt[5]

1 – Dartmouth College
2 – Georgia Institute of Technology
3 – Woods Hole Oceanographic Institution
4 – Brown University
5 – Cornell University

Contents of this file

Additional Supporting Information (Files uploaded separately)

Introduction

The following supplementary material contains an extended discussion of the multiphase evolution of the roofs and floors of sills simulated and discussed within the main manuscript and discusses the influence of reservoir chemistry and thermal driving on the thicknesses and propagation rates of these interfaces (Text S1). Figure S1 depicts the temporal evolution (growth) of sill floors and roofs during sill solidification. Figure S2 depicts the chemical evolution (salination) of the residual liquid reservoir during sill solidification. Captions for Movies M1-M33 describe the simulations these supporting .avi movies depict.

Text S1 – Sill Roof and Floor Evolution

During solidification the physicochemical properties and propagation rates of the multiphase 'mushy layers' that characterize the ice-brine interfaces of the roofs and floors of sills evolve. This evolution is dependent on the thermal gradients driving the solidification as well as the chemical composition of the sill. In Figure S1 we show the temporal evolution (growth) of the roof and floor mushy layers of the two sills (35 ppt NaCl and 35 ppt $MgSO_4$) we simulated in the main manuscript as well as the roof and floor mushy layer evolution of two additional sill simulations (1 – a freshwater (0 ppt) sill subject to the same thermal driving as the sills in the main manuscript and 2 – a 35 ppt NaCl sill with symmetric undercooling of 132 K at both the top and bottom boundary). These simulations were carried out to investigate the impacts environmental conditions (e.g., thermal driving, initial reservoir chemistry) have on mushy layer and sill roof/floor evolution. In three of the simulations, we track the ice-mush (IM) phase boundary as well as the mush-liquid (ML) phase boundary for both the roofs and floors of the sills. The space between these two phase boundaries defines the mushy layer – where a nonzero brine volume fraction exists. There does not exist a mushy layer in the freshwater sill (an expected result of freezing a pure fluid [*Huber et al.*, 2008; *Rubinšteĭn*, 2000]) so only the ML phase boundary is shown and represents a sharp ice-water transition.

Several expected trends are apparent in Figure S1 including 1) larger undercoolings lead to faster interface propagation; 2) floors have thicker mushy layers than roofs (consistent with our conclusions in the main manuscript); 3) mushy layers thin near the end of the sill solidifications as the residual fluid concentrates; and 4) mushy layers in $MgSO_4$ systems are much thinner than those of NaCl systems. Another less intuitive trend is also evident – the similar propagation rate of the freshwater sill roof and the ML interfaces of comparably undercooled saline sills, which sometimes even exceed the rate of the freshwater sill. While somewhat counterintuitive, given the freezing point depression effects of a saline/concentrating sill, ML interface propagation is primarily driven by conductive heat loss to the cold adjacent ice [*Buffo et al.*, 2021a], which can continue to be efficient in the ice phase of the mushy layer. Brine convection within the mushy layer may also amplify the efficiency of heat loss from the liquid reservoir, potentially explaining the ML propagation rates that exceed those of the freshwater roof. Interestingly, the ML interface propagation of the sill floor outpaces that of the sill roof in the symmetric undercooling case (dashed blue line and solid blue line of Figure S1, respectively). This suggests that while brine convection in the roof mushy layer amplifies heat loss from the residual reservoir it also acts to cycle relatively warm water into the roof mushy layer from the reservoir, slowing its ML interface propagation in relation to the floor ML interface.

In the end these comparative simulations show that both thermal driving and reservoir chemistry play a role in governing mushy layer thicknesses – shallower thermal gradients lead to thicker mushy layers and mushy layer thickness is proportional to the freezing point depression effects of solutes (i.e., NaCl results in thicker mushy layers as it has a much low eutectic temperature and saturation point). Conversely, while thermal driving plays a large role in governing mushy layer interface propagation rates (interface propagation rates are proportional to the magnitude of the driving thermal gradient) salinity plays a much smaller role and minimally impacts the rate of the ice-liquid/mush-liquid interface (additional tests with nonzero salinities distinct from the 35 ppt values used in the current simulations would need to be carried out to determine the effect of salinity on the propagation rates of the IM interface).

Environmental conditions (e.g., thermal environment, brine chemistry) have significant impacts on the structure, dynamics, and evolution of ice-brine interfaces on icy worlds throughout the solar system, including Earth [*Feltham et al.*, 2006; *Hunke et al.*, 2011]. Given the importance of these interfaces in governing the evolution of planetary ice shells and any internal hydrological features they may contain as well as their integral role in mediating material and heat transport between planetary hydrospheres and cryospheres [*Buffo et al.*, *2020; Vance et al.*, 2016; *Vance et al.*, 2020], constraining the physicochemical properties and dynamics of ice-brine mushy layers will play a fundamental role in improving our understanding and predictive modeling capabilities of ice-ocean world geophysics, habitability, and spacecraft mission observations (see discussions in *Buffo et al.* [2021b] and *Vance et al.* [2020]).

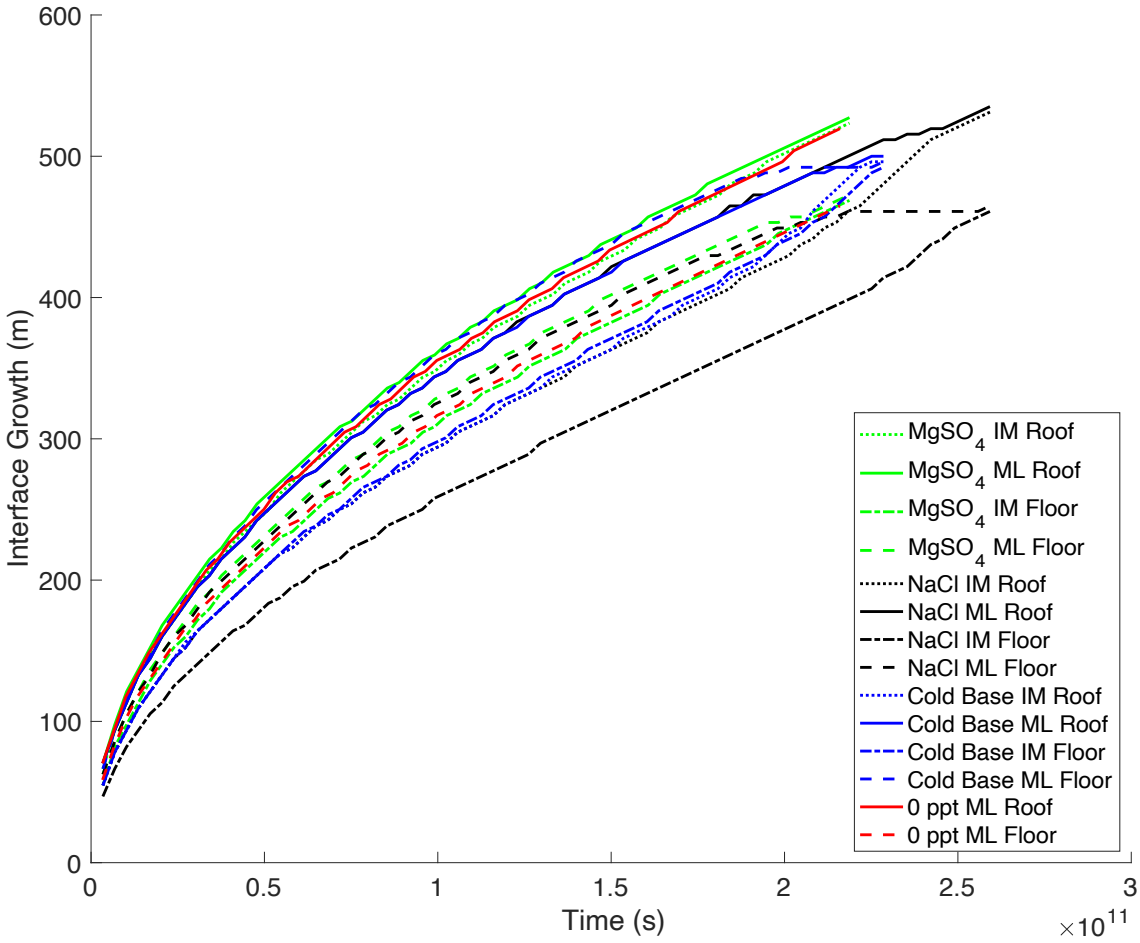

Figure S1. The growth of sill floor and roof mushy layers. The temporal propagation of the key interfaces that define the mushy layers of sill floors and roofs are plotted for all four simulations described in Text S1. Lines labeled as '$MgSO_4$' and 'NaCl' represent results from the 35 ppt sill simulations described in the main manuscript. Lines labeled as 'Cold Base' represent results from a 35 ppt NaCl sill solidification simulation driven by symmetric Dirichlet thermal forcing at its upper and lower boundaries of 132 K. Lines labeled as '0 ppt' represent results from the solidification of a freshwater sill subject to the same thermal forcing describe in the main manuscript. 'IM' signifies the ice-mush interface – the transition between a solid below the eutectic (porosity = 0) and the mushy layer (porosity >0), and 'ML' signifies the mush-liquid interface – the transition between the mushy layer and the reservoir fluid (porosity = 1).

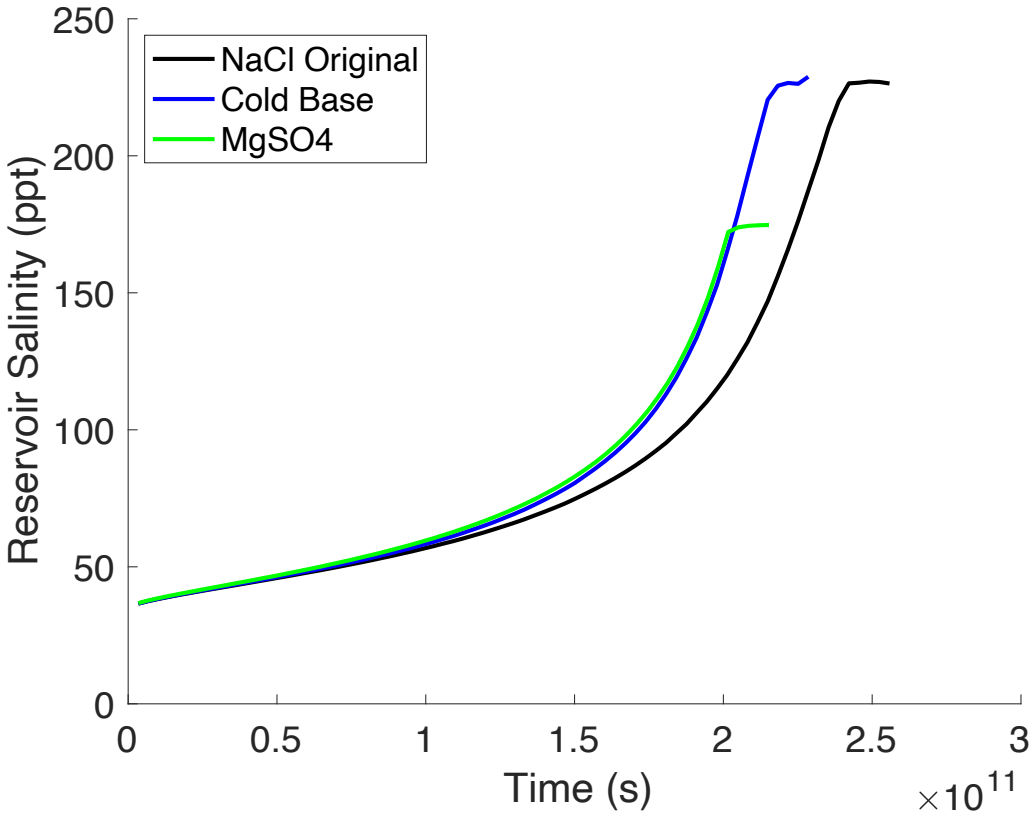

Figure S2. Salination of solidifying sills. As isolated sills freeze brine is rejected from the mushy layers of their roofs, concentrating their residual liquid reservoir. The temporal evolution of this process is shown for three different simulations. The plateaus near the end of the run correspond to the eutectic concentrations of the respective sills.

Movie S1. Bulk salinity evolution of a 1 km thick 35 ppt NaCl sill subject to the undercooling boundary conditions presented in Figure 2. Black contours demarcate porosities ranging from 0.15 to 0.95 in increments of 0.2.

Movie S2. Porosity evolution of a 1 km thick 35 ppt NaCl sill subject to the undercooling boundary conditions presented in Figure 2.

Movie S3. Streamline evolution of a 1 km thick 35 ppt NaCl sill subject to the undercooling boundary conditions presented in Figure 2. Streamlines are represented as blue to red contours that indicate relative flow speed along the streamline.

Movie S4. Bulk salinity evolution of a 1 km thick 35 ppt $MgSO_4$ sill subject to the undercooling boundary conditions presented in Figure 2. Black contours demarcate porosities ranging from 0.15 to 0.95 in increments of 0.2.

Movie S5. Porosity evolution of a 1 km thick 35 ppt $MgSO_4$ sill subject to the undercooling boundary conditions presented in Figure 2.

Movie S6. Streamline evolution of a 1 km thick 35 ppt $MgSO_4$ sill subject to the undercooling boundary conditions presented in Figure 2. Streamlines are represented as blue to red contours that indicate relative flow speed along the streamline.

Movie S7. Bulk salinity evolution of a 1 m by 1 m 35 ppt NaCl ocean filled fracture subject to the undercooling boundary conditions presented in Figure 2 (200 K undercooling). Black contours demarcate porosities ranging from 0.15 to 0.95 in increments of 0.2.

Movie S8. Porosity evolution of a 1 m by 1 m 35 ppt NaCl ocean filled fracture subject to the undercooling boundary conditions presented in Figure 2 (200 K undercooling).

Movie S9. Streamline evolution of a 1 m by 1 m 35 ppt NaCl ocean filled fracture subject to the undercooling boundary conditions presented in Figure 2 (200 K undercooling). Streamlines are represented as blue to red contours that indicate relative flow speed along the streamline.

Movie S10. Bulk salinity evolution of a 10 m by 20 m 35 ppt NaCl ocean filled fracture subject to the undercooling boundary conditions presented in Figure 2 (200 K undercooling). Black contours demarcate porosities ranging from 0.15 to 0.95 in increments of 0.2.

Movie S11. Porosity evolution of a 10 m by 20 m 35 ppt NaCl ocean filled fracture subject to the undercooling boundary conditions presented in Figure 2 (200 K undercooling).

Movie S12. Streamline evolution of a 10 m by 20 m 35 ppt NaCl ocean filled fracture subject to the undercooling boundary conditions presented in Figure 2 (200 K

undercooling). Streamlines are represented as blue to red contours that indicate relative flow speed along the streamline.

Movie S13. Bulk salinity evolution of a 100 m by 200 m 35 ppt NaCl ocean filled fracture subject to the undercooling boundary conditions presented in Figure 2 (200 K undercooling). Black contours demarcate porosities ranging from 0.15 to 0.95 in increments of 0.2.

Movie S14. Porosity evolution of a 100 m by 200 m 35 ppt NaCl ocean filled fracture subject to the undercooling boundary conditions presented in Figure 2 (200 K undercooling).

Movie S15. Streamline evolution of a 100 m by 200 m 35 ppt NaCl ocean filled fracture subject to the undercooling boundary conditions presented in Figure 2 (200 K undercooling). Streamlines are represented as blue to red contours that indicate relative flow speed along the streamline.

Movie S16. Bulk salinity evolution of a 500 m by 1000 m 35 ppt NaCl ocean filled fracture subject to the undercooling boundary conditions presented in Figure 2 (200 K undercooling). Black contours demarcate porosities ranging from 0.15 to 0.95 in increments of 0.2.

Movie S17. Porosity evolution of a 500 m by 1000 m 35 ppt NaCl ocean filled fracture subject to the undercooling boundary conditions presented in Figure 2 (200 K undercooling).

Movie S18. Streamline evolution of a 500 m by 1000 m 35 ppt NaCl ocean filled fracture subject to the undercooling boundary conditions presented in Figure 2 (200 K undercooling). Streamlines are represented as blue to red contours that indicate relative flow speed along the streamline.

Movie S19. Bulk salinity evolution of a 1 m by 1 m 35 ppt $MgSO_4$ ocean filled fracture subject to the undercooling boundary conditions presented in Figure 2 (200 K undercooling). Black contours demarcate porosities ranging from 0.15 to 0.95 in increments of 0.2.

Movie S20. Porosity evolution of a 1 m by 1 m 35 ppt $MgSO_4$ ocean filled fracture subject to the undercooling boundary conditions presented in Figure 2 (200 K undercooling).

Movie S21. Streamline evolution of a 1 m by 1 m 35 ppt $MgSO_4$ ocean filled fracture subject to the undercooling boundary conditions presented in Figure 2 (200 K undercooling). Streamlines are represented as blue to red contours that indicate relative flow speed along the streamline.

Movie S22. Bulk salinity evolution of a 10 m by 20 m 35 ppt $MgSO_4$ ocean filled fracture subject to the undercooling boundary conditions presented in Figure 2 (200 K

undercooling). Black contours demarcate porosities ranging from 0.15 to 0.95 in increments of 0.2.

Movie S23. Porosity evolution of a 10 m by 20 m 35 ppt $MgSO_4$ ocean filled fracture subject to the undercooling boundary conditions presented in Figure 2 (200 K undercooling).

Movie S24. Streamline evolution of a 10 m by 20 m 35 ppt $MgSO_4$ ocean filled fracture subject to the undercooling boundary conditions presented in Figure 2 (200 K undercooling). Streamlines are represented as blue to red contours that indicate relative flow speed along the streamline.

Movie S25. Bulk salinity evolution of a 100 m by 200 m 35 ppt $MgSO_4$ ocean filled fracture subject to the undercooling boundary conditions presented in Figure 2 (200 K undercooling). Black contours demarcate porosities ranging from 0.15 to 0.95 in increments of 0.2.

Movie S26. Porosity evolution of a 100 m by 200 m 35 ppt $MgSO_4$ ocean filled fracture subject to the undercooling boundary conditions presented in Figure 2 (200 K undercooling).

Movie S27. Streamline evolution of a 100 m by 200 m 35 ppt $MgSO_4$ ocean filled fracture subject to the undercooling boundary conditions presented in Figure 2 (200 K undercooling). Streamlines are represented as blue to red contours that indicate relative flow speed along the streamline.

Movie S28. Bulk salinity evolution of a 500 m by 1000 m 35 ppt $MgSO_4$ ocean filled fracture subject to the undercooling boundary conditions presented in Figure 2 (200 K undercooling). Black contours demarcate porosities ranging from 0.15 to 0.95 in increments of 0.2.

Movie S29. Porosity evolution of a 500 m by 1000 m 35 ppt $MgSO_4$ ocean filled fracture subject to the undercooling boundary conditions presented in Figure 2 (200 K undercooling).

Movie S30. Streamline evolution of a 500 m by 1000 m 35 ppt $MgSO_4$ ocean filled fracture subject to the undercooling boundary conditions presented in Figure 2 (200 K undercooling). Streamlines are represented as blue to red contours that indicate relative flow speed along the streamline.

Movie S31. Bulk salinity evolution of a 500 m by 1000 m 35 ppt NaCl ocean filled fracture subject to the undercooling boundary conditions presented in Figure 2 (260 K

undercooling). Black contours demarcate porosities ranging from 0.15 to 0.95 in increments of 0.2.

Movie S32. Porosity evolution of a 500 m by 1000 m 35 ppt NaCl ocean filled fracture subject to the undercooling boundary conditions presented in Figure 2 (260 K undercooling).

Movie S33. Streamline evolution of a 500 m by 1000 m 35 ppt NaCl ocean filled fracture subject to the undercooling boundary conditions presented in Figure 2 (260 K undercooling). Streamlines are represented as blue to red contours that indicate relative flow speed along the streamline.

References

Buffo, J., B. Schmidt, C. Huber, and C. Meyer (2021a), Characterizing the Ice-Ocean Interface of Icy Worlds: A Theoretical Approach, *Icarus*.

Buffo, J., B. Schmidt, C. Huber, and C. Walker (*2020*), Entrainment and dynamics of ocean-derived impurities within Europa's ice shell, *JGR: Planets*.

Buffo, J. J., C. R. Meyer, J. R. Parkinson, and B. E. Schmidt (2021b), Dynamics of a solidifying icy satellite shell, *JGR: Planets*.

Feltham, D. L., N. Untersteiner, J. S. Wettlaufer, and M. G. Worster (2006), Sea ice is a mushy layer, *Geophysical Research Letters*, *33*(14), doi:Artn L14501 10.1029/2006gl026290.

Huber, C., A. Parmigiani, B. Chopard, M. Manga, and O. Bachmann (2008), Lattice Boltzmann model for melting with natural convection, *International Journal of Heat and Fluid Flow*, *29*(5), 1469-1480, doi:10.1016/j.ijheatfluidflow.2008.05.002.

Hunke, E. C., D. Notz, A. K. Turner, and M. Vancoppenolle (2011), The multiphase physics of sea ice: a review for model developers, *Cryosphere*, *5*(4), 989-1009, doi:10.5194/tc-5-989-2011.

Rubinšteĭn, L. (2000), *The stefan problem*, American Mathematical Soc.

Vance, S. D., K. P. Hand, and R. T. Pappalardo (2016), Geophysical controls of chemical disequilibria in Europa, *Geophysical Research Letters*, *43*(10), 4871-4879, doi:10.1002/2016gl068547.

Vance, S. D., B. Journaux, M. Hesse, and G. Steinbrügge (2020), The Salty Secrets of Icy Ocean Worlds, *Journal of Geophysical Research: Planets*, e2020JE006736.